THE MASS AND STRUCTURE OF THE REMNANT OF TYCHO'S SUPERNOVA

Paul Gorenstein, Frederick Seward, and Wallace Tucker
Harvard/Smithsonian Center for Astrophysics,
Cambridge, MA 02138

ABSTRACT

A high resolution X-ray image of Tycho's supernova remnant obtained from the Einstein Observatory reveals three components of X-ray emission that we identify with shocked interstellar material, diffuse ejecta, and clumpy ejecta. This picture is applied to derive the mass of X-ray emitting material. Assuming a distance of 3 kpc, an absorbing column density of 3×10^{21} atoms/cm^2, and using an ion-electron non-equilibrium calculation for the emissivity, we find the average density of the ISM is 0.4 atoms/cm^3, and the energy contained in the remnant is 1.4×10^{51} ergs. The total mass of X-ray emitting material in the remnant is $\approx 4\ M_\odot$, $\approx 2\ M_\odot$ ejecta and $\approx 2\ M_\odot$ swept up, putting the remnant at an intermediate state between a free expansion and the Sedov phase. There is no evidence for neutron star. The upper limit on the surface temperature is in the range 1.1 to 1.8×10^6K.

1.0 INTRODUCTION

The remnant of the supernova explosion of 1572 described by Tycho (Brahe 1573, Clark and Stevenson 1977) occupies a unique and important position in the study of SNRs. The age of the remnant is known, and the light curve was well-measured (Baade 1945) and firmly establishes the supernova as type I. Indeed, when a "typical" example of a type I SN is mentioned in the literature, it is usually Tycho's. Information concerning the mass of ejecta in this SNR are therefore vital to determining the nature of the type I SN explosion.

Much of the recent theoretical work has centered on low mass stars as progenitors of Type I SN. A number of authors (Arnett 1979, Chevalier 1981, Nomoto 1981, and Wheeler 1982) have considered accreting white dwarfs of $\sim 1.5 M_\odot$ which are disrupted completely by the explosion, leaving no compact remnant and producing a large amount of Ni 56. In a more general way, Lasher (1975) showed that the narrowness of the peak of the early Type I SN light curve required $\lesssim 2 M_\odot$ of ejecta. This is

J. Danziger and P. Gorenstein (eds.), Supernova Remnants and their X-Ray Emission, 1–15.

consistent with the observed lack of correlation of Type I supernovae with spiral arms which points to an older stellar population of low mass stars (see, e.g., Maza and van den Bergh 1976). On the other hand, Oemler and Tinsley (1979) have argued that Type I supernovae are correlated with star formation rates and are therefore associated with stars having lifetimes less than about a billion years, or masses greater than about two solar masses. Weaver, Axelrod and Woosley (1980) have shown how the evolution of a 9 $M_\odot$ star can lead to a Type I supernova event. So, the question as to the mass of the progenitor remains open.

Another approach to this problem is to study the dynamics of the remnant. Strom, Goss and Shaver (1982) have recently made an important contribution in this connection. Using two radio maps taken eight years apart, they have shown that the expansion velocity of Tycho's SNR is 3600 ± 360 km/s at a radius of 221 arc seconds or 0.99×10^{19} cm, assuming a distance of 3 kpc. This is to be compared with the average velocity of expansion which is 7640 km/sec over the 410 year lifetime of Tycho's SNR. The ratio of the present to the average velocity is $0.47\pm.044$, in agreement with the results of Kamper and van den Bergh (1976) which were based on optical observations. These results have generally been taken as proof that Tycho's supernova remnant is in the adiabatic phase, with the swept-up mass much greater than the ejected mass. In this phase the radius $R \propto t^{2/5}$, so the velocity $\dot{R} = V = \frac{2}{5}\frac{R}{t} = 0.4\ \bar{V}$. However, a comparison of the instantaneous and average velocities of expansion may be misleading if a reverse shock (McKee 1974) is present. The reverse shock, moving back into the expanding ejecta, appears to an external observer to be expanding at a lower velocity than the primary shock propagating into the ISM. If the reverse shock is bright, the observed expansion will be closer to that of the reverse shock than that of the shock in the ISM.

Yet another approach is to attempt to infer the mass by means of X-ray observations. All heated material is visible through its X-ray emission. The observed morphology, a model for the three-dimensional structure, and the measured X-ray surface brightness and temperature can be used to calculate the amount of X-ray emitting plasma. Spectra taken with the Einstein SSS (Becker et al. 1980) show surprisingly strong emission lines, particularly from Si and S. Both equilibrium and non-equilibrium models require several times solar abundance of Si group elements (Shull 1982a). The spectrum obtained from HEAO-1 (Pravdo et al. 1980) shows X-ray emission to at least 25 keV, requiring high temperatures in at least part of the remnant. An Einstein IPC observation was reported by Reid, Becker and Long (1982) based upon substantially lower spatial resolution than the HRI measurements. They derive a mass of X-ray emitting material of $15M_\odot$ and a density of 2.3 atoms/cm^3 for the ISM, typical of past results for this remnant. The better resolution of the HRI, a lower value of interstellar absorption, and a recent non-equilibrium emissivity calculation lead to an ISM density of only 0.4 (this paper) and to a lower calculated mass of the remnant. The X-ray luminosity is consistent with this lower mass

because of high emissivity from non-equilibrium effects, enrichment of metal abundances, and the presence of clumps in the ejecta.

In the following sections, we will show that the high resolution Einstein image has features which can be interpreted as a shock heated shell in the ISM and an inner shell containing ejecta which has broken into clumps. The mass of plasma in each region will be calculated from the observed surface brightness using emissivities generated from a model in which ions and electrons are not in equilibrium. The result places the remnant in a phase intermediate between a free expansion and the Sedov phase.

2.0 THE EINSTEIN HRI OBSERVATION

2.1 Overview

The Einstein telescope was pointed at Tycho's SNR for 22 hours starting 1940 UT, 8 February 1979. The resulting image contained 14 hours of good data and is shown in Figure 1 at various levels of exposure. Several features are apparent:

(1) The remnant is almost circular with diameter of 8 arcminutes. There is limb brightening, not uniform around the circumference but indicative of emission from a shell, which varies from a maximum in the NW to a minimum in the SE where there is almost no limb brightening at all. There is a discontinuity in the SE which is exactly that observed in the radio region (Duin and Strom 1975, Dickel et al. 1982).

(2) A thin shelf of emission can be seen at the outer edge of the remnant, outside the region of maximum brightness, around most of the circumference. We assume that this feature is produced by radiation from a shock wave propagating into the interstellar medium. The interstellar shock wave is clearest on the west side and the circles shown in Figure 1D are centered with respect to this outer shock.

(3) There is no emission detected from a central compact object or from any point-like source within the remnant.

(4) Most of the emission is from small, irregular, patchy regions. These must be clumps of material having high X-ray luminosity either because of greater-than-average density or greater-than-average emissivity. Temperature variations will also affect the brightness but not as strongly. We assume that this material is supernova ejecta. These clumps appear to be arranged inside a spherical shell (with the exception of the SE discontinuity), but the distribution within the shell is far from uniform. Individual clumps can be discerned in the center of the remnant (where we are looking approximately normal to the surface of the shell) and in the SE where the density of clumps is low. Maximum surface brightness of the remnant is in the NW, where the density of clumps is highest. The brightest regions are due to limb brightening from many overlapping high emissivity clumps.

https://doi.org/10.1017/S0074180900033611 Published online by Cambridge University Press

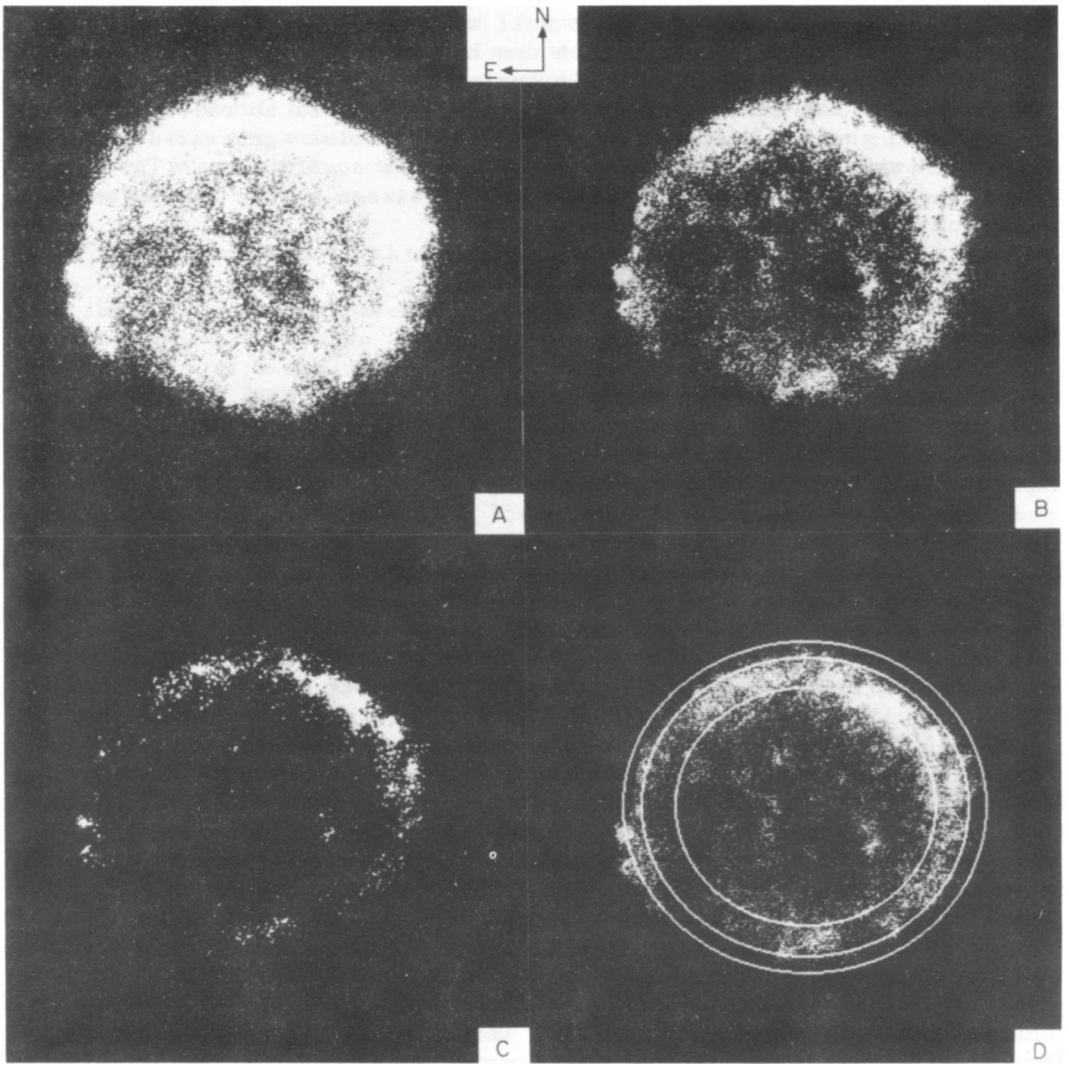

Figure 1: The Einstein HRI image of Tycho's SNR exposed to show (A) the faint shock heated material on the outside of the remnant, (B) the clumpy appearance of the X-ray emitting material, and (C) the brightest regions around the limb. (D) Circles with radii 172", 216", and 240" are centered at RA $0^h22^m30^s9$, Dec $63^o51'45"$. These illustrate the two shells described in the text.

https://doi.org/10.1017/S0074180900033611 Published online by Cambridge University Press

2.2 Details

The HRI image of a point source consists of a high resolution core FWHM ~4 arcseconds and a rather broad tail several arcminutes in extent due to scattering from imperfections in the mirrors. At 2 keV, 45% of the focused energy is contained in a circle of diameter 12 arcseconds, and this fraction decreases as photon energy increases. The effect of scattering appears in the image as an increased brightness in the center of the remnant and as faint diffuse emission outside the shell. Figure 2 is a contour plot of an image that has been deconvolved by a maximum entropy technique.

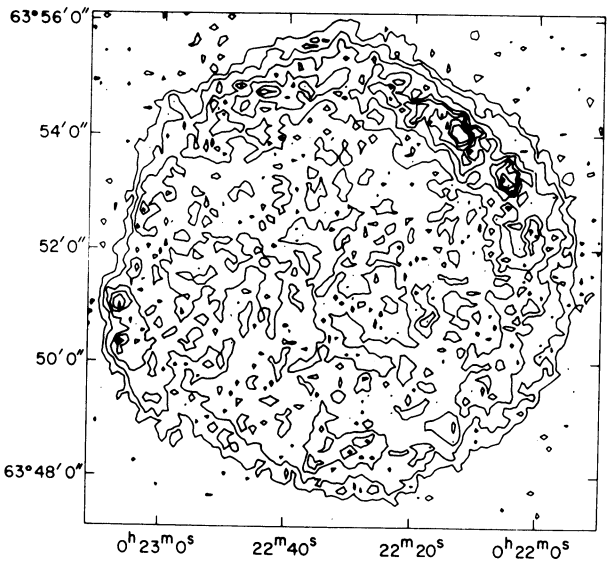

Figure 2: Contour map of Tycho. The spacing between the contours of constant surface brightness is 1×10^{-5} HRI counts/s.arcsec^2 except that the spacing of the first two contours is half this.

Figure 3 shows radial profiles of surface brightness (prior to deconvolution) for 12 equal segments, each spanning 30° in position angle. It illustrates the gross clumpiness in the interior of the remnant and the variation in limb brightening around the circumference. The center of these radial profiles is RA $0^h22^m30^s.9$, Dec 63°51′45″ as illustrated in Figure 1D. The maximum extent is exhibited by the SE discontinuity at PA 90°–120°, and the minimum extent by the adjoining region at PA 150°–180°. The shock appears in some of these profiles as a small inflection superimposed on the generally smooth decrease in surface brightness going outward from maximum emission at the limb. The gradually decreasing background starting at a radius of 4 arcminutes is due to the scattering wings of the instrument response. Variations in the radius of the remnant over the 30° segments, certainly over the 360° average, wash out the characteristic structure associated with the shock. Figures 1, 2, and 3 may be compared with the IPC data given by Reid et al. (1981) which have a resolution of ~1.5 arcmin. The IPC is more sensitive than the HRI at higher X-ray energy. The basic features of the remnant are the same in the IPC and in the HRI image implying that there are no gross spectral differences in emission from different

https://doi.org/10.1017/S0074180900033611 Published online by Cambridge University Press

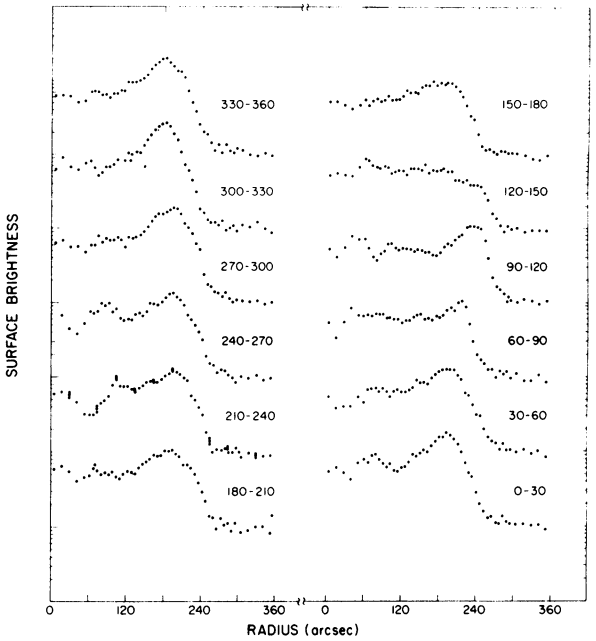

Figure 3: Surface brightness as function of radius at 12 different position angles.

parts of the remnant. The resolution of the IPC was not good enough to distinguish the shock or the clumps of material. Maximum limb brightening measured in the NW with the HRI is ≈4 compared with ≈2.5 with the IPC. Figure 4 shows surface brightness averaged over only 10° in position angle centered at position angles of 235° and 315° (measured from N through E) where the shock is prominent. The HRI response to a uniform ring of inner and outer radii 156″ and 204″ (an approximation to the projection of a shell) is shown as a solid curve. Note that the broad wings of the HRI response to this ring (containing 90% of the emission) contribute considerable brightness over the rest of the remnant. These data are from the HRI image with no deconvolution and show the strength of the various signals and backgrounds. After subtraction of background due to instrument response to the bright limb, we calculated surface brightness of the shock and from the interior. Since densities to be calculated depend on the square root of the surface brightness, small uncertainties in background subtraction are not important.

3.0 MASS DISTRIBUTION MODEL

The high resolution image allows us to identify three components of the X-ray emission: (1) emission from an outer shell of radius R_0 = 240″ and thickness $\Delta R/R \sim .1$; this we identify with shocked interstellar matter; (2) emission from diffuse material in a shell of outer radius $R_1 \approx 216''$ and thickness $\Delta R/R \sim 0.2$; this we identify with supernova ejecta; (3) emission from clumps distributed in the same shell as the diffuse ejecta; this we also identify with supernova ejecta. The contribution of these three components is summarized in Table 1.

https://doi.org/10.1017/S0074180900033611 Published online by Cambridge University Press

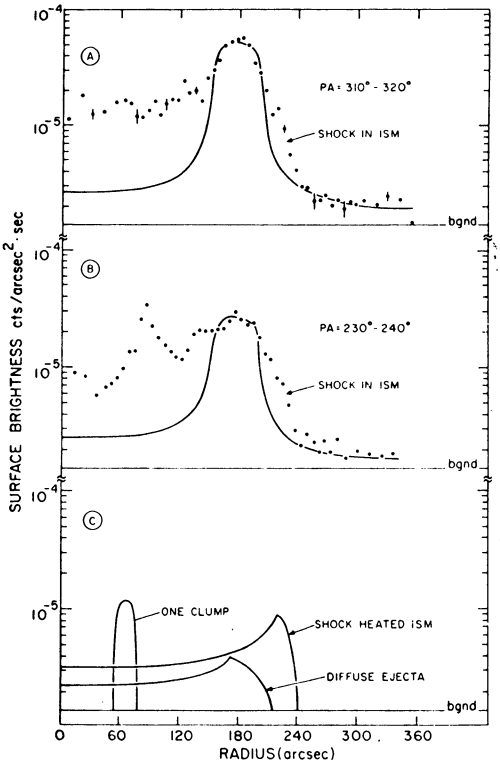

Figure 4: Surface brightness at 2 position angles, one with maximum limb brightening, one with a very bright clump. Solid curve shows instrument response to bright ring of emission. Solid curves in lower plot show surface brightness of shell of shock heated material, inner shell of diffuse emission and of a typical clump. Lower curves refer only to source, instrument response is not included.

Table 1. Data From HRI Image

Region	Surface Brightness (counts/s.arcsec^2)	Geometry	Signal (counts/s)
shock	7.4 (-6) at limb	shell r_o=240" r_i=216"	0.80
diffuse ejecta	0.8 (-6) at center	shell r_o=216" r_i=173"	0.21
one clump	10.3 (-6) at maximum	sphere r=12"	0.0047
all clumps		400 distributed in diffuse ejecta shell	1.86
total remnant			2.87

https://doi.org/10.1017/S0074180900033611 Published online by Cambridge University Press

We use the observed surface brightness of the shock to calculate the swept up mass, M_s, and density of the ISM. We then calculate the ejecta mass, M_e, and compare the ratio of M_e/M_s with that determined from the measured dynamic state of the SNR. The shock in the ISM is assumed to be spherical, and composed of material of normal cosmic abundance that has been snowplowed and heated by the shock to a temperature which is dependent on the shock velocity. At the end of the next section, we will deduce a shock velocity $\approx$6000 (d/3 kpc), implying a temperature of $\approx 4 \times 10^8$K = 36 keV. The high energy X-rays detected by Pravdo and Smith (1979) imply the existence of some high temperature material but do not support the bulk of shock heated material being at 36 keV. A lower temperature gives a better fit to the high energy spectrum, and we use a temperature of 7 keV. This is consistent with the idea that the electrons and ions have yet to come to equilibrium, so that the electron kinetic temperature is lower than the ion kinetic temperature (Itoh 1977).

As can be seen in Figure 1, 70% of the detected X-rays come from a clumpy shell just behind the shock heated material. We assume this shell contains the stellar debris or ejecta which has been greatly enhanced in silicon group elements as required by the X-ray spectrum (Becker et al. 1980, Shull 1982a). The ejecta (or ejecta-containing regions) are clumpy and the size distribution of clumps can be estimated from the X-ray image.

The observed clumps are not uniform, and the distribution in size can be estimated from the central part of the remnant where isolated clumps are observed. Since no unresolved point sources appear, clump dimensions can be measured. We approximate the actual distribution with two components: uniform density clumps with diameter 24" (0.34 pc), and a uniform distribution of material filling a shell of outer radius 216" and of thickness 0.2 of this radius.

4.0 CALCULATION OF SWEPT UP AND EJECTA MASS

We take the distance to the remnant as 3 kpc. Estimates in the literature range between 2 and 6 kpc, and recent references are briefly reviewed by Strom et al. (1982) and Reid et al. (1982). The dependence of calculated mass on distance, d, is $d^{5/2}$. Thermal energy also goes as $d^{5/2}$, and kinetic energy is proportional to $d^{9/2}$. Using the model described above (i.e. 2 shells of diffuse emission plus clumps), the X-ray surface brightness observations can be used to calculate density of material in the different components of the remnant and hence their mass. The major uncertainties in the calculation concern the emissivity of the plasma and the absorption of X-rays in the ISM between the SNR and Earth. The ISM column density is taken as 3×10^{21} atom/cm^2 with solar composition. This is the neutral H absorption measure of Hughes, Thompson and Colvin (1971). If the column density were doubled to 6×10^{21} atoms/cm^3, our calculated masses would increase by 30-40%. Considerations of ionization, recombination, and expansion time scales indicate that the ions and electrons are not in

https://doi.org/10.1017/S0074180900033611 Published online by Cambridge University Press

thermal equilibrium (Itoh 1977). The shock heated electrons probably achieve equilibrium, but the ions are collisionally ionized more slowly and "ionization" temperature lags behind electron temperature which lags behind the ion kinetic temperature. Shull (1982a) has calculated the emissivity of a Sedov model for Tycho's SNR containing an enriched plasma (abundances of elements relative to solar are 0.4 (Ne), 2 (Mg), 8 (Si), 6 (S), 3 (Ar), 3 (Ca), and 2 (Fe)) and shock heated to an (electron) temperature of 7 keV. Parameters were adjusted to fit the SSS spectral data. We have used these emissivities under the assumption that emissivity of the Sedov model is approximately that of the recently shocked material. Shull (1982b) has also kindly provided an identical calculation for material of solar composition.

The electron density, n, in a diffuse, thin source of thermal X-rays can be calculated from the observed surface brightness using the expression

$$n^2 = 5.35 \times 10^{11} \frac{1}{H} \frac{\varepsilon}{T_r P(T)} S \frac{1}{t}.$$

S is observed surface brightness in counts/arcsec^2.sec; t is depth of emitting region in cm; T_r is transmission of ISM and has value <1; P(T) is emissivity in the .2-4 keV band of 1 cm^3 of plasma in ergs cm^3/s; ε is detector efficiency in erg/cm^2/count; and H is a factor, varying between 1.0 for a point source and 2.0 for a large diffuse source, which takes into account the spatial response function of the detector.

The mass, M, and X-ray luminosity, L_x, depend on the density and volume, V, of the source

$$M = \mu n V \text{ and } L_x = n^2 P(T) V,$$

where μ is the average ion mass per electron and n is the number of electrons/cm^3.

4.1 Swept-up Mass

We first calculate the parameters of the interstellar shock. Subtraction of HRI background and instrument response to the bright inner ring gives the surface brightness of shocked material at the point of maximum limb brightening within the shocked ISM. Since it is generally accepted that the gas behind the shock is not in equilibrium, we use the non-equilibrium solar calculations of Shull (1982b) for the emissivity. The density in the shock heated ISM is found to be 1.44 cm^{-3}. Assuming a compression factor of 3.7 behind the shock ($\Delta R/R = 0.10$), the ambient interstellar electron density is 0.39 cm^{-3}, corresponding to a baryon density N = 0.50 cm^{-3}. The swept up mass is 2.2 $M_\odot$.

https://doi.org/10.1017/S0074180900033611 Published online by Cambridge University Press

4.2 Diffuse Component of Ejecta Shell

The diffuse component of the ejecta shell is determined by the minimum measured surface brightness at the center of the remnant. There are regions in the center, apparently free of clumps, which have a residual brightness after subtraction of the HRI response to the bright regions in the rim of the remnant and subtraction of the contribution of the shocked ISM shell. Assuming that (a) this material is distributed in a shell of outer radius R_c = 216″ and thickness $\Delta R/R = 0.2$, (b) the emissivity is given by the non-equilibrium enriched calculation of Shull (1982a), we calculate an electron density of 0.61 cm^{-3} and a mass of 1.2 $M_\odot$. If we assume that the temperatures of the electron and ion components in the diffuse shell are the same as in the swept up material, then the pressure in the diffuse ejecta shell is less than in the shell of swept up material, consistent with the idea that the ejecta shell is decelerating.

4.3 Clumpy Ejecta

The measured size and surface brightness of a few individual clumps were used to calculate the average characteristics of a clump. The remaining emission of the remnant, after subtracting contributions of the shock and the diffuse ejecta, was entirely assigned to clumps with no restrictions on the arrangement of the clumps within the remnant. The density of the clumpy ejecta, assuming a non-equilibrium plasma enriched in silicon group elements, and pressure equilibrium between the diffuse and clumpy ejecta, is found to be 2.5 cm^{-3}. The mass of the clumpy ejecta is 0.7 $M_\odot$. Pressure equilibrium fixes the temperature of the material in clumps at 2 keV. Table 2 summarizes the masses derived for the different components. For comparison with previous work, and to illustrate two other possibilities (which at present are not thought to be as likely as the non-equilibrium model), we have included in the table results from an equilibrium calculation with slightly enriched ejecta and super-enriched ejecta.

The ejecta mass resulting from an equilibrium calculation with temperatures derived from the SSS spectrum (Becker et al. 1980) is 3.6 $M_\odot$. The only way of reducing this mass considerably is to assume that the ejecta are bright in X-rays, not because their density is high, but because the emissivity is high. The emissivity can be increased by increasing the abundance of the medium heavy elements by a large factor. For example, if it is assumed that the medium heavy elements are enhanced by a factor of 1000, then the emissivity will be enhanced by a factor of about 10–100 depending on temperature (cf., Long, Dopita, and Tuohy 1982). The computed ejecta mass would then be reduced to 1.4 $M_\odot$, and the ratio of swept up to ejected mass would be about 4. There are two difficulties with this approach. First, if we increase the emissivity by too large a factor, then the computed density will be low, and the clumps would not be in pressure equilibrium with the surrounding gas, so it is difficult to see how they could exist. Second, if the mass of the ejecta gets too small, the SNR would be in the Sedov phase,

Table 2. Calculated Physical Parameters

Region	Material	Assumed Temp. (keV)	0.2-4 keV P(T) (ergs cm^3/s)	n (elec/cm^3)	μ	Mass ($M_\odot$)	0.2-4 keV L_x (ergs/s)
			Non-equilibrium				
shock	non-equilibrium solar	7.	7 (-23)	1.44	1.3	2.2	1.9 (35)
diffuse ejecta	non-equilibrium enriched[a]	7.	10 (-23)	0.61	1.3	1.2	0.7 (35)
ejecta clumps	non-equilibrium enriched[a]	2.	20 (-23)[b]	2.5	1.3	0.7	3.1 (35)
			Ionization Equilibrium				
shock	solar	5.	1.2 (-23)	3.2	1.3	5.0	1.8 (35)
diffuse ejecta	enriched[a]	5.	2.4 (-23)	1.15	1.3	2.3	0.6 (35)
ejecta clumps	enriched[a]	0.5	5.6 (-23)	4.6	1.3	1.3	3.1 (35)
			Ionization Equilibrium and Super-enriched Ejecta				
shock	solar	5.	1.2 (-23)	3.2	1.3	5.0	1.8 (35)
diffuse ejecta	metal abundance 1000 x solar	5.	2.4 (-22)	0.36	2.0	1.1	0.6 (35)
ejecta clumps		0.5	2.5 (-21)	0.68	2.0	0.3	3.1 (35)

[a]Elemental enrichment relative to solar are: 0.4(Ne), 2(Mg), 8(Si), 3(Ar), 3(Ca), and 2(Fe) after Shull, 1982a.

[b]Emissivity assumed to scale $\propto T^{-1/2}$ between 7 and 2 keV.

https://doi.org/10.1017/S0074180900033611 Published online by Cambridge University Press

the ejecta would be well mixed with swept up ISM, and we would not expect to see the two-shell structure that we see. In summary, it seems that the observations of the spatial structure constrain the mass of ejecta to be approximately equal to that of the swept up mass, and favor a non-equilibrium model in which the medium heavy abundances are enhanced only about an order of magnitude.

The non-equilibrium results given in Table 2 show that the mass of the ejecta is approximately equal to the mass of the swept up matter. This means that Tycho is in a stage intermediate between uniform expansion and the adiabatic phase. Theoretical work on the dynamics of supernova remnants indicates that this intermediate stage is characterized by: (1) a shock wave moving into the interstellar medium with a velocity v_s (Rosenberg and Scheuer 1973); (2) a reverse shock wave moving back into the ejecta with a velocity less than v_s (McKee 1974, Chevalier 1982a,b); and (3) clumps of material created by instabilities in the decelerating ejecta (Gull 1975; Jones, Smith, and Straker 1981).

This theoretical picture is not far from what is observed in the high resolution X-ray image of the Tycho SNR. The observed ratio of radii of the reverse and interstellar shock waves is 0.72, compared with 0.77 derived from Chevalier (1982b). Chevalier (1982a) calculates the density profile of a shock and reverse shock in a young SNR expanding into a uniform radius. Our observation is close to this, but the shocked ejecta shell is about three times as thick as his calculation, extending more both towards the ISM shock and back toward the center of the remnant. We attribute this to the breakup of the ejecta shell into clumps as calculated by Gull (1975) and, as expected, the size of the observed clumps is comparable with the thickness of the reversed-shocked shell. The theoretical work is not detailed enough to satisfactorily calculate the energy and velocities from our data. Rosenberg and Scheuer (1973) calculate the propagation of a shock into a uniform ISM. By scaling Tycho's apportioned remnant to their work at $M_{ej} = M_{sw}$, we derive $E_o = 1.4 \times 10^{51}$ ergs, 0.2×10^{51} ergs thermal and 1.2×10^{51} ergs kinetic. The velocity of the shock in the ISM is 6000 km/s, and the velocity of the material behind the shock as well as the contact discontinuity (the surface between the shocked ISM and the shocked ejecta) is 4500 km/s. On the other hand, Chevalier assumes that the ISM shock velocity is $\propto t^{4/7}$ or 4700 km/s for Tycho's SNR and, at the present time, ($t = 1.28\ t_c$ in his notation) the velocity of the reverse shock is 2700 km/s.

The expansion velocities of 3000-3600 km/sec as measured by Strom et al. (1982) in radio and by Kamper and van den Bergh (1978) in the optical (when adjusted to a 3 kpc distance) is consistent with our analysis, if we interpret these measurements as referring to the shocked ejecta or pre-existing material and not to the interstellar shock wave. It appears that most radio emission is from the region we identify with the diffuse ejecta shell (Dickel et al. 1982). Thus, it is likely that the velocity of the ISM shock is considerably greater than the radio

expansion velocity and that the remnant is not as close to the Sedov phase as they have concluded. The bright optical filaments are found in regions where the outermost radial contour is at a local minimum in distance from the center of Tycho. They may correspond to regions where the shock has encountered pre-existing interstellar material. We suggest that the expansion velocities that are seen are those of accelerated interstellar material rather than of the primary shock. In fact, we might expect the brightest and most conspicuous optical and radio filaments to occur under these local conditions and not be indicative of the higher global velocity of the interstellar shock.

The ejected mass of 1.9 $M_\odot$ is somewhat larger than the value of 1.4 $M_\odot$ expected from exploding white dwarf models (Chevalier 1981 and references). However, a small reduction in the assumed distance would bring the computed mass below 1.4 $M_\odot$, so this discrepancy is perhaps not serious. On the other hand, an increase in distance or in absorbing ISM column density will increase the mass considerably above this theoretical expectation.

5.0 NO NEUTRON STAR DETECTED

Since no point sources were detected inside the remnant, we can set an upper limit to the surface temperature of a neutron star which may have been formed in the explosion. We consider two positions: at the center where the surface brightness is low, and as a pessimistic upper limit, the bright knot ~1.5' N of the center. The 3σ upper limit to the signal of a point source at the center is 30 counts. If the source were located in the bright knot, the signal could be as high as 90 counts. There are several such knots or clumps inside this remnant. None appear as unresolved point sources, and there are no features which might distinguish one of them as containing a compact object. The upper limit to the surface temperature was calculated by folding black body spectra as observed through the ISM and the detector response over a range of temperatures. The radius of the neutron star was assumed to be 11 km. The limit is also dependent on the distance and column density of ISM. At a distance of 3 kpc, the limit ranges from 1.1×10^6K ($N_H = 3 \times 10^{21}$, center) to 1.8×10^6K ($N_H = 9 \times 10^{21}$, knot). The significance of this has been discussed at length by Nomoto and Tsuruta (1981) and by Van Riper and Lamb (1981).

6.0 SUMMARY

A high resolution X-ray image of the Tycho SNR reveals three emission components:

(1) an outer shell of radius 240", $\Delta R/R \approx 0.1$,
(2) a diffuse inner shell of radius 216", and
(3) ~400 bright clumps of material distributed in a shell of radius 216", $\Delta R/R \approx 0.2$.

https://doi.org/10.1017/S0074180900033611 Published online by Cambridge University Press

We identify these components with

(1) shocked interstellar matter,
(2) diffuse supernova ejecta, and
(3) clumpy supernova ejecta.

The mass of these components is calculated to be 2.2 $M_\odot$, 1.2 $M_\odot$ and 0.7 $M_\odot$, respectively.

The swept up mass is approximately equal to the ejected mass, so Tycho's SNR must be a stage intermediate between the uniform expansion and adiabatic stages. The observed morphology of the remnant is in reasonable agreement with theoretical expectations, but no numerical calculations have been published showing the reverse shock at this stage of evolution. The mass estimates scale as the distance according to $d^{5/2}$, so a reduction from the assumed distance of 3 kpc to 2.5 kpc would reduce the ejected mass to 1.4 $M_\odot$.

At a distance of 3 kpc, the upper limit on the surface temperature of a central neutron star is found to be in the range 1.1 to 1.8 million degrees.

REFERENCES

Arnett, W.D. 1979, Ap.J. (Letters), 230, L37.
Baade, W. 1945, Ap.J., 96, 188.
Becker, R.H., Holt, S.S., Smith, B.W., White, N.E., Boldt, E.A., Mushotzky, R.F., and Serlemitsos, P.J. 1980, Ap.J., 235, L5.
Brahe, T. 1573, De Nova Stella, Laurentius Benedictus Copenhagen, 1573. Facsimile Edition, Danish Royal Scientific Society, Copenhagen, 1901.
Chevalier, R. 1981, Ap.J., 246, 267.
Chevalier, R. 1982a, Ap.J., 258, 790.
Chevalier, R. 1982b, Ap.J. (Letters), 259, L85.
Clark, D.H. and Stevenson, F.R. 1977, The Historical Supernovae, (Pergamon Press, Oxford).
Dickel, J.R., Murray, S.S., and Morris, J. 1982, Ap.J., 257, 145.
Duin, R.M. and Strom, R.G. 1975, Ast. and Ap., 39, 33.
Gull, S.F. 1975, MNRAS, 171, 263.
Hill, R.W., Burginyon, G.A., and Seward, F.D. 1975, Ap.J., 200, 158.
Hughes, M., Thompson, A., and Colvin, R. 1971, Ap.J. Suppl., 23, 323.
Itoh, H. 1977, Pub. Ast. Soc. Japan, 29, 813.
Jones, E.M., Smith, B.W., and Straker, W.C. 1981, Ap.J., 249, 185.
Kamper, K.W. and van den Bergh, S. 1978, Ap.J., 224, 851.
Lasher, G. 1975, Ap.J., 201, 194.
Long, K.S., Dopita, M.A., and Tuohy, I.R. 1982, Columbia Astrophysics Laboratory preprint #213.
Maza, J. and van den Bergh, S. 1976, Ap.J., 204, 519.
McKee, C. 1974, Ap.J., 188, 335.
Nomoto, K. 1981, in Fundamental Problems in the Theory of Stellar Evolution, ed. D. Sugimoto, D.Q. Lamb, and D.N. Schramm (Dordrecht:Reidel) p. 295-315.

Nomoto, K. and Tsuruta, S. 1981, Ap.J. (Letters), 250, L19.
Oemler, Jr., A. and Tinsley, B.M. 1979, A.J., 84, 985.
Pravdo, S.H. and Smith, B.W. 1979, Ap.J. (Letters), 234, L195.
Pravdo, S.H., Smith, B.W., Charles, P.A., and Tuohy, I.R. 1980, Ap.J. (Letters), 235, L9.
Reid, P.B., Becker, R.H. and Long, K.S. 1982, Ap.J., 261, 485.
Rosenberg, I. and Scheuer, P.A.G. 1973, MNRAS, 161, 27
Shull, J.M. 1982a, Ap.J. (Letters) (in press, Vol. 262).
Shull, J.M. 1982b, private communication.
Strom, R.G., Goss, W.M., and Shaver, P.A. 1982, MNRAS, 200, 473.
Van den Berg, S., Marscher, A.P., and Terzian, Y. 1973, Ap.J. Suppl., 26, 19.
Van Riper, K.A. and Lamb, D.Q. 1981, Ap.J. (Letters), 244, L13.
Weaver, T.A., Axelrod, T.S., and Woosley, S.E. 1980, in Proc. Texas Workshop on Type I Supernovae, ed. J.C. Wheeler (Austin: University of Texas Press), p. 113.
Wheeler, J.C. 1982, in Proc. NATO Advanced Study Institute on Supernovae (Cambridge: Institute of Astronomy), p. 167.

DISCUSSION

KIRSHNER: Is there a problem with clumps that might be present on a scale smaller than your resolution? Would it be possible to get away with less mass if the material were clumpy on all scales?

GORENSTEIN: If there were clumps smaller than our resolution, we would mistake them for diffuse emission and overestimate the mass. However, there is no reason to believe they exist because the typical clump we do see is several times larger than our resolution.

DICKEL: Could some of the clumps be overtaken interstellar ones which are now evaporating rather than lumps of ejection?

GORENSTEIN: The clumps are probably responsible for the enrichment in Si, S, Ca, and A. This indicates that they are primaily ejecta.

CHEVALIER: Were the non-equilibrium calculations used in the mass estimates consistent with most of the emission coming from the reverse shock region?

GORENSTEIN: We used the non-equilibrium ionization model of Shull which is obtained by fitting the theory to the SSS intensity and spectrum of Tycho. We did not consider a complete non-equilibrium model that provides an independent prediction for the X-ray intensity of the reverse shock.

WINKLER: Why have you taken the temperature of the inner diffuse shell of ejecta to be the same (7 keV) as that of the outer shell of ISM?

GORENSTEIN: This was an assumption. However, the value of the mass is relatively insensitive to temperature.